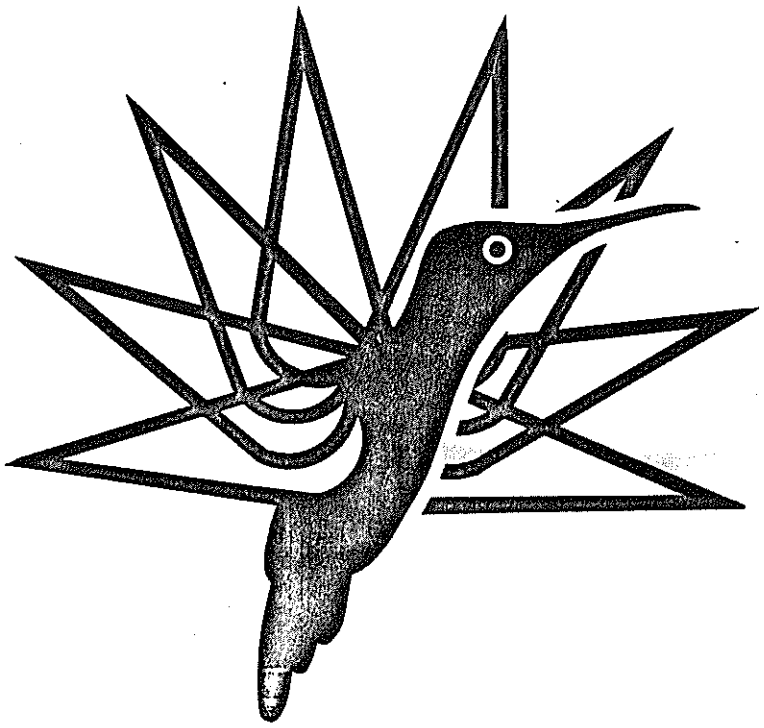

AN ANALYSIS OF HELICOPTER ROTORHEAD DRAG BASED ON NEW EXPERIMENT

by

J. Seddon
Aeronautical Consultant;
Senior Research Fellow, University of Bristol

FIFTH EUROPEAN ROTORCRAFT AND POWERED LIFT AIRCRAFT FORUM
SEPTEMBER 4 – 7TH 1979 - AMSTERDAM, THE NETHERLANDS

AN ANALYSIS OF HELICOPTER ROTORHEAD DRAG BASED ON NEW EXPERIMENT

by

J. Seddon
Aeronautical consultant;
Senior Research Fellow, University of Bristol

ABSTRACT

It was considered that the nature of rotorhead drag, including the various aerodynamic interferences that contribute to it, was insufficiently understood. A wind tunnel experiment has therefore been made with the aims of (a) relating the drag to the classical drag of a circular cylinder across the stream and (b) extracting the interferences in suitable analytical form. The results of the experiment are condensed into a simple formula, which it is suggested may be applied generally to unfaired rotorheads.

NOTATION

A_p	Projected frontal area of head
A_z	Area allowance for fuselage boundary layer
A_s	Area addition for flow spoiling on canopy
C_D	Drag coefficient, $D/q_\infty A_p$
C_p	Static pressure coefficient, p/q_∞
D	Drag force
f(s/w)	Function for flow spoiling with canopy Y, Fig. 11
h	Height of canopy
ℓ	Length of canopy from head position to trailing edge
p	Static pressure referred to free stream value
q	Local dynamic pressure, $\frac{1}{2}\rho V^2$
q_∞	Free stream dynamic pressure, $\frac{1}{2}\rho V_\infty^2$
s	Distance between canopy surface and rotorhead arms
V	Velocity
V_∞	Free stream velocity
w	Width of canopy
α	Factor to allow for azimuth variation
ρ	Density of air

1. Introduction

The conventional helicopter rotorhead, consisting of a central vertical hub, a set of horizontal arms (inboard of the lifting blades) and any additional items which are separately exposed (control rods, etc.), is an important source of parasitic drag. An illustration of this is provided in reference 1, where a breakdown of parasitic drag is given for a typical single-rotor helicopter. The sources of drag are there listed as basic fuselage, landing gear, main rotorhead, nacelles, roughness leaks and cooling, and miscellaneous. Among these the rotorhead drag comes out as being:-

the largest single item;
or 22% of the total parasitic drag;
or 1·75 times the basic fuselage drag;

which is an impressive if somewhat daunting reckoning. The example relates to an articulated rotor: with a hingeless or semi-rigid rotor the head drag is normally somewhat lower but still a large component. More important perhaps than the need to reduce the drag of a given arrangement is the need to be able to estimate it in the early stages of design, since it is then that consideration of the various factors involved can be most usefully set alongside the many other design considerations.

Sheehy[2] has made a review of American data, in which it is shown, inter alia, that the rotorhead as installed in the vehicle carries a significantly higher drag penalty than would the same head in isolation at the same flight speed; in other words, that the juxtaposition of rotorhead and vehicle normally gives rise to a large interference drag. Analysis of this interference drag is not attempted in Sheehy's paper, beyond a comment that a value of local dynamic pressure 25% in excess of the free stream value would generally fall short of accounting for it. The results collected by Sheehy exhibit considerable variation, depending on canopy configuration and possibly other factors.

To obtain a basic understanding of at least the primary factors which determine both the isolated drag of a typical rotorhead and also the interference drag when installed in typical fashion was the object of the present study. In a number of aspects, Sheehy's review provided the starting point needed for the present work.

2. Prior examination

The study is concerned essentially with unfaired heads. Figure 1 shows Sheehy's collected results for installed head drag (Fig. 4 of ref. 2) plotted together with a number of results obtained by Westland Aircraft Ltd in the past few years: these latter are from wind tunnel model tests of rotorhead assemblies relating to various helicopter projects. Installed head drag is plotted as a function of head frontal area* and Sheehy's empirical approximation to the basic drag of heads

* This is the maximum projected area, i.e. the frontal area as defined with one pair of arms set across the stream in the case of a four-bladed rotor.

when measured in isolation is shown as a full line. There is clearly a good correspondence between the Westland results and Sheehy's collection; and Sheehy's point that interference drag (the difference between installed and isolated drag) is generally more than 25% of the basic isolated drag is substantiated.

The fact that head frontal area is the dominant parameter indicates that the flow is a type of bluff body flow, characterised by boundary layer separation and a turbulent wake. Since the elementary shapes making up the head tend to be of high aspect ratio (cross-stream length divided by cross-stream thickness) the classical analogue is the flow around an infinite-span circular cylinder. In the present work this analogy has been used in preference to exploring Sheehy's empirical approximation shown in Fig. 1. Any generalisations following from the circular cylinder approach clearly need to take Reynolds number considerations into account.

The interference drag may be regarded as consisting of two parts:-

(a) additional drag on the head itself resulting from its presence in the flow field of the helicopter fuselage, and

(b) any additional drag on the fuselage (including the canopy) resulting from flow spoiling produced by the head.

Part (a) may itself have more than one component. The two components which can most readily be anticipated are:-

(a.1) change of drag due to the supervelocity field of the fuselage;

(a.2) change of drag due to part immersion of the central hub in the fuselage boundary layer.

Part (b) relates to any failure to achieve the same pressure recovery on rearward-facing surfaces of the fuselage as would be achieved by the flow in absence of the head. This will depend on canopy configuration and possibly other features such as the rear fuselage upsweep. The experiment which follows was designed to separate out and separately assess these various components of the interference drag.

Two factors which the Sheehy review shows to be relatively unimportant are the effect of Mach number and the effect of head rotation. In each case, convincing evidence is given and both these conclusions are entirely reasonable. Concerning the effect of rotation it may be noted that on the head itself, angular velocities are everywhere small compared with the forward speed in flight conditions for which drag is important. Some variation in drag may be expected, however, with position in azimuth of a non-rotating head and this parameter is relatively easy to include in an experiment.

3. Nature of experiment

Based on this prior examination, the present experiment was set up to do the following:-

Check the breakdown between basic (i.e. isolated) head drag and interference drag.

Correlate the drag with fuselage pressure plotting.

Vary the shape of canopy on which the head was mounted.

Examine the flow and pressure distribution over the rear fuselage upsweep.

Check the effect of head azimuth angle (non-rotating).

At a later stage it was found desirable to investigate the drag breakdown between rotor arms and central hub and also the effect of boundary layer on the mounting surface. Additional pressure measurements were made in the stream away from the fuselage surface and fuselage boundary layer thicknesses at the head position were also measured, for the different arrangements.

A $^1/_5$ scale helicopter model was made available by Westland Aircraft for the tests: this is shown in Fig. 2. Two model rotorheads (each for 4-blade rotor) were provided. Head A, used for the main analysis, was the more basically simple shape, consisting of a cylindrical central hub and cylindrical arms in three sections of different diameter (Fig. 3). Head B was a relatively complex model (Fig. 4) the shapes of both hub and arms being more representative of actual detail: detachable control rods were also provided in this case. Thus it was possible to check that conclusions drawn from analysing the simpler shape could be applied also to a more detailed representation. The central hub of head A could be tested without the arms: this condition is termed head C. Heads A and C could be used with four different heights of the central hub, denoted by the numbers 1 to 4. Thus the total set of head arrangements available comprised the following:-

Heads A1 to A4 (i.e. varying height)

Heads B1 and B2 (i.e. without and with control rods)

Heads C1 to C4 (i.e. central hub of A, varying height)

The standard canopy of the helicopter model as provided was of complex shape (Fig. 5), featuring a front lip, a well in which the rotorhead was mounted and a pair of unfaired engine jet exits at the rear. This model was used only sparingly and is labelled canopy Z. For the main analysis, a smooth streamlined canopy model (canopy Y, Fig. 6) was made, having the same overall proportions as canopy Z, together with a further model (canopy X) giving virtually a minimum faired shape from the top of the aircraft cabin to the tail boom - an unrealistic ideal but providing a datum case for analysis of the canopy effects.

In order to assess firstly the isolated head drag and secondly the effect of fuselage boundary layer, a flat board was provided, having the plan shape of the helicopter model and a similar three-

point support in the tunnel. The model heads were mounted on this board (a) with adequate spacers for the isolated drag tests and (b) directly for measurement of the boundary layer effect, varying heights of the central hub being used in both cases.

The experiment was conducted in the 7 ft. x 5 ft. low speed wind tunnel of the Aeronautical Engineering Department of Bristol University, at various times during the period June to October 1978.

4. Results and discussion

The results of the experiment are now discussed in a sequence intended to build up the overall picture one element at a time, starting with the isolated head drag.

4.1 Isolated head drag

Using the flat board mounting with spacers, the method was to add spacers successively until the drag increment of the head reached a constant value: this ensured that the head was clear of the effect of boundary layer on the flat board. The results of Table 1 below were then obtained.

Table 1: Drag of heads in isolation

Head	D/q_∞, ft^2	A_p, ft^2	C_D
A2	3·24	3·32	0·98
A3	3·12	3·15	0·99
B1	2·99	3·27	0·91
B2	3·80	3·94	0·96
C2	0·92	1·16	0·79
C2 plus one spacer	1·62	2·07	0·78

The drag coefficient of approximately 1·0 for head A is consistent with the classical result for a circular cylinder; since the Reynolds numbers of the elements of the head at model scale range from 8×10^4 to 2×10^5 and correspond therefore to the high end of the subcritical range ($C_D \sim 1{\cdot}2$) and the start of the critical fall in C_D. In the case of head B1, the rather lower value of C_D is explained by the fact that with this head, the inboard ends of the arms are progressively faired (Fig. 4), so that locally the circular cylinder analogue does not hold. The higher C_D given by head B2 is then accounted for by the fact that addition of the pitch change levers spoils this fairing

somewhat, together with the fact that all the control rods are relatively low Reynolds number elements. Finally, the drag coefficient of about 0·8 for head C is consistent with the rest, since the central hub has the highest Reynolds number of all the elements, which therefore takes it some way into the critical range.

4.2 Surface boundary layer effect

When the heads were mounted directly on to the flat board, i.e. without spacers, the head drag was significantly lower than the corresponding value in Table 1. This is attributable to the central hub being partly immersed in the boundary layer of the mounting surface. The results for heads A and C mounted in this way, with varying heights of the hub, are plotted in Fig. 7. It is seen that a good fit to the experimental results is given by straight lines corresponding to C_D = 1·0 and 0·8, for heads A and C respectively, emanating from a common point on the horizontal axis at a positive value (A_Z) of the frontal area. This value may be regarded as the area of hub which is given a "free ride" as a consequence of the base of the hub being immersed in the boundary layer of the mounting surface. A useful confirmation of this analysis is provided by the results for heads A and C in isolation (Table 1): when plotted directly against frontal area A_p they lie distinctly above the lines in Fig. 7, but if plotted at area values ($A_p + A_Z$), they conform well (see flagged symbols) with the other data.

The overall result at this stage, therefore, is that in a uniform pressure field at free stream velocity (as provided by the flat board), the head drag may be expressed in the form:

$$D/q_\infty = C_D (A_p - A_Z) \qquad \ldots\ldots (1)$$

in which C_D is the classical drag coefficient for a circular cylinder at equivalent Reynolds number.

4.3 Supervelocity effect

Turning now to tests with the helicopter model, Figs. 8a and b show streamwise surface pressure distributions over the canopies X and Y, measured along the centre lines. The distributions with head absent indicate the supervelocity fields in which the head is located: the distributions with head present show the pressure rise ahead of the hub prior to boundary layer separation and a high level of suction in the wake immediately behind the hub.

The centre line distributions were augmented by similar measurements along parallel lines off centre and also by measurements away from the surface along a vertical line corresponding to the rotor axis (with head absent). From this total evidence values were deduced for mean supervelocity of the flow at the head position: in dynamic pressure terms, these compare with the centre-line surface values of Fig. 8 as shown in Table 2.

Table 2: Supervelocity fields

Canopy	Local $q \div q_\infty$ (head absent)	
	centre-line surface	mean for head position
X	1·30	1·24
Y	1·52	1·45

4.4 Total interference drag

The head drags with canopies X and Y are shown in Fig. 9. The main results are for head A: results for heads B and C give additional support, however, when these are factored to a value $C_D = 1{\cdot}0$, using Table 1. The further analysis is in two parts:-

(i) For canopy X (the datum shape), a good fit of the points is obtained by assuming the same value of A_z as for the flat board tests - check measurements of the boundary layer thicknesses for both canopies justified this - and applying the factor 1·24 for local dynamic pressure from Table 2, together with $C_D = 1{\cdot}0$. Thus it appears that the supervelocity effect (a.1 of the discussion in Section 2) is present in full. At the same time, the result conforms to there being no reverse interference of the head on the canopy drag (item b. of Section 2), which is as expected since the surface of the datum shape lies virtually wholly along the free stream direction, so that normal-pressure drag is automatically zero.

(ii) Applying a similar analysis to the measurements with canopy Y, it is seen that the dynamic pressure factor, 1·45 from Table 2, does not in this case account for the whole drag. We may conclude that a further drag component arises from spoiling of the flow over the rear of the canopy by the presence of the head. That flow spoiling is in fact present is confirmed by the pressure distributions in Fig. 8b, where it is seen that the pressure distribution with head in place fails to achieve the recovery towards the canopy trailing edge which is shown in the distribution with head removed: the lower pressures in this region of rearward-facing surface thus constitute the interference drag in question. Examination of the flow with tufts showed that with the head in place, the flow was very disturbed, though not actually separated. It would presumably be possible, given a more abrupt

canopy rear shape, for the flow to separate behind the head, but remain attached when the head was not present: this would result in a still greater interference of type b. than that shown.

It is convenient to represent the type b. interference in terms of an effective increase A_s of head frontal area as shown in Fig. 9. The total installed drag of the head may now be written:-

$$D/q = C_D (A_p - A_z + A_s) \quad \ldots\ldots (2)$$

where q is the local dynamic pressure, defined by the flow field of fuselage and canopy with head absent. The overall interference drag (installed drag minus isolated drag) is thus a combination of the factors q/q_∞ (type a.1), A_z (type a.2) and A_s (type b.).

4.5 Effect of azimuth angle

The results so far described all relate to the head being mounted with one pair of arms directly across the stream. In any other fixed azimuth position the head drag is reduced somewhat, as may be seen in Fig. 10 where results for various head and canopy combinations are plotted in the form of head drag, ratioed to the drag at zero azimuth, versus azimuth angle. From 45° to 90° the variation is virtually an image of that from 0° to 45°. No significant discrimination between cases is observed and it is seen that the mean drag over 360° azimuth variation is approximately 92% of that at zero azimuth. This puts a further factor into the drag equation which now becomes

$$D/q = \alpha C_D (A_p - A_z + A_s) \quad \ldots\ldots (3)$$

where α is the azimuth factor, here assessed as having the value 0·92.

4.6 Flow over rear fuselage upsweep

It was thought initially that aerodynamic interference might occur between the disturbed flow created by the head and the flow over the rear fuselage upsweep, which latter might itself be in a sensitive state, particularly at nose-down angles of the fuselage. The situation was investigated (at zero yaw only) both by visual inspection of flow tufts and also by extensive pressure plotting of the rear fuselage, at zero angle of attack and also at 9° nose down. No such interference could be discerned: the pressure distributions with any of the heads, mounted on canopy Y which was reckoned to give the most interference-prone situation, were effectively identical with corresponding distributions with the head removed.

5. Generalisation of results

Following on from the foregoing analysis, it is suggested that rotorhead drag for unfaired heads may generally be expressed

in the form given by equation (3), Section 4.5 above. For general application of the formula, some further consideration of the factors that have been introduced is required.

Beginning with the isolated drag, an appropriate value of C_D must be selected. Basically C_D is Reynolds number dependent and an estimate needs to be made using a standard reference (for example Ref. 3) for the classical cylinder flow. The question of surface roughness needs to be considered: this has not been studied carefully in the present context but generally one might expect the roughness levels at full scale to be such as to both restrict the magnitude of the critical fall in C_D and also accelerate the subsequent rise in the supercritical regime: in the end therefore it seems likely that the effective value of C_D will be not greatly different from 1·0. It may further be noted that Sheehy[2] comments that small scale model tests tend to undervalue the full scale drag of an unfaired head, probably because of the difficulty of accurately modelling the head details. The overall scale effect question is thus one on which more comparative data are desirable.

The azimuth factor α, on a basis of the present evidence, is effectively independent of head details, whether the head is isolated or installed, and may be taken as having the value 0·92 in all cases.

Turning to the interference factors, chief of these is the local supervelocity, which may be estimated by either analytical or computational methods. The remaining factors are the corrections to effective projected area, A_Z and A_S.

5.1 The factor A_Z

Measurements were made of boundary layer thickness on the flat board and on the helicopter fuselage with each of the canopies X and Y. All three tests gave approximately the same thickness (with head removed), which when multiplied by the width of the central hub at base (the same for all heads) gave an area 0·21 ft^2 at full scale. The value of A_Z shown in Figs. 7, 9 is slightly greater than this, the difference however being within the possible errors of determination of both the boundary layer thickness, by experiment, and the A_Z value by curve-fitting. It is concluded that the "free ride" area A_Z is roughly equal to the area of hub up to one boundary layer thickness (defined in absence of the hub) from the mounting surface. This is probably accurate enough for most estimation purposes.

5.2 The factor A_S

The factor A_S, representing the effect of flow spoiling over the rear of the canopy, is a function of canopy shape and also of proximity of the arms of the head to the surface of the canopy. Deduced values of A_S/A_D are plotted in Fig. 11 in terms of a separation ratio s/w: with canopy X the interference factor is effectively zero, as already shown; with canopy Y the factor is seen to decrease as separation ratio increases. Note that the total head drag increases nevertheless with increase of separation ratio (Fig. 9) because of the dominant effect of head frontal area.

As regards the dependence of A_S upon canopy profile, one may suggest as a first approximation a direct proportionality to the effective height/length of the canopy aft of the head (Fig. 12). For canopy Y the value of h/ℓ is 0·23: if therefore the variation shown in Fig. 11 is represented by the function f(s/w), the overall variation suggested for the general case is

$$\frac{A_S}{A_p} = 4{\cdot}4 \frac{h}{\ell} \cdot f\left(\frac{s}{w}\right) \qquad \ldots\ldots (4)$$

If the canopy embodies bluff areas at the rear (e.g. engine exits) where the airflow would separate whether the head were present or not, such areas must be excluded in defining an effective value of h/ℓ. Canopy Z is a case in point, having an overall value of h/ℓ in excess of that of canopy Y, but an effective value only 0·17. The experiment showed that the flow spoiling drag produced by either head A or head B was less with canopy Z than with canopy Y.

5.3 Partial test of formula

A test of the interference components in the general formula can be made by estimating from it the drag of heads B1 and B2 in combination with canopy Z, since no analytical measurements were made for canopy Z because of its complex shape. Details of the calculation are given in Table 3.

Table 3: Drag of heads B1 and B2 with canopy Z

Item	B1	B2	Remarks
C_D	0·91	0·96	From Table 1
A_p, ft^2	2·82	3·49	Ignores area screened by well
A_Z, ft^2	0·21	0·21	
s/w	0·25	0·25	
f(s/w)	0·11	0·11	From Fig. 11
h/ℓ	0·17	0·17	Based on aft line ignoring jet area
A_S, ft^2	0·08	0·08	From eqn. (4)
D/q, ft^2	2·43	3·61	
q/q_∞	1·45	1·45	Assumed same as for canopy Y
D/q_∞	3·55	4·68	From eqn. (2)
"	3·61	4·75	Measured

6. Summary and conclusions

Whilst it was well appreciated that rotorhead drag forms a large part of the parasitic drag of a helicopter, the nature of that drag, and of the aerodynamic interferences which contribute to it, was not sufficiently understood.

A wind tunnel experiment has therefore been made with the aims of

(a) relating the drag to the classical drag of an infinite cylinder lying across the airstream;

(b) extracting in analytical form the interference of the fuselage flow field on the rotorhead drag and the inverse interference of flow spoiling produced by the rotorhead on the fuselage drag.

Results of the analysis are summarised in equation (3) - Section 4 - which contains the various factors relating to the aims at (a) and (b) above.

It is suggested that equation (3) may be used as a general expression for calculating the drag of unfaired rotorheads and notes are added - Section 5 - to assist the practical application.

The paper does not discuss the benefits and problems of fairing the head, for which the reader is referred elsewhere - for example, to Reference 2.

REFERENCES

1) Keys, Wiesner; Parasite drag; JAHS Vol 20 No 1 1975

2) T.W. Sheehy; A general review of helicopter rotor hub drag data; Paper presented at the Stratford AHS Chapter Meeting, December 1975

3) - ; Fluid forces acting on circular cylinders for application in general engineering; ESDU Data Sheets 70013, 70014

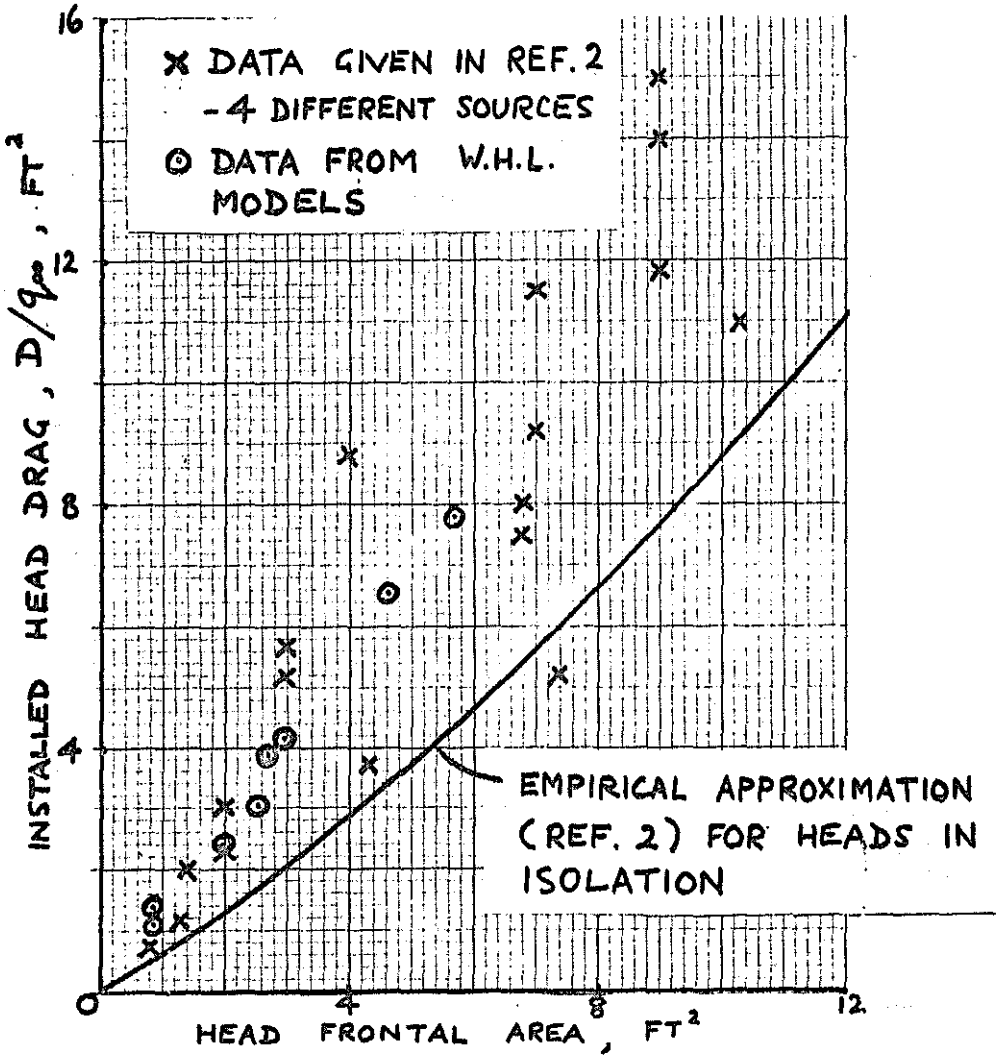

FIG. 1 COLLECTED DATA, REF. 2 & WHL

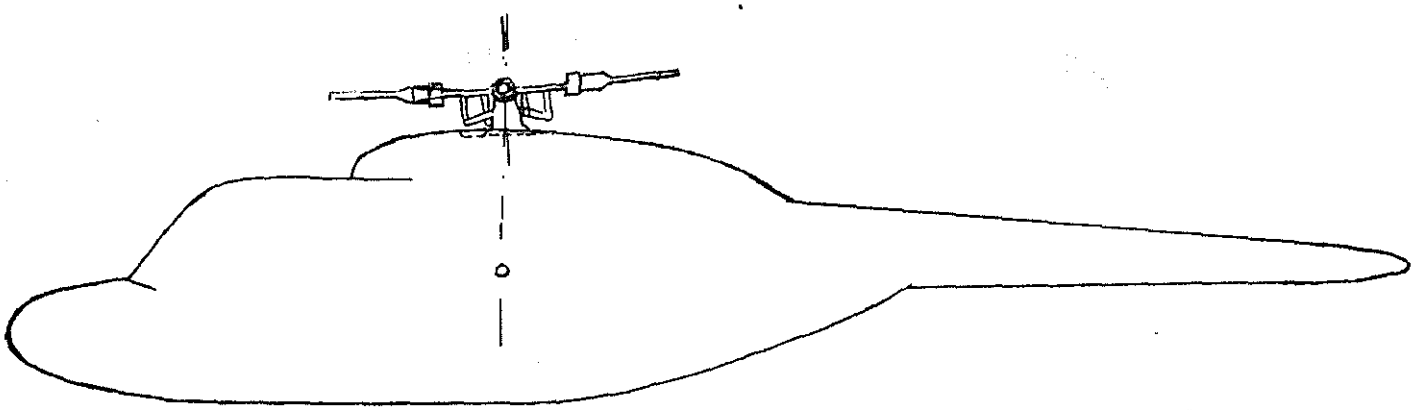

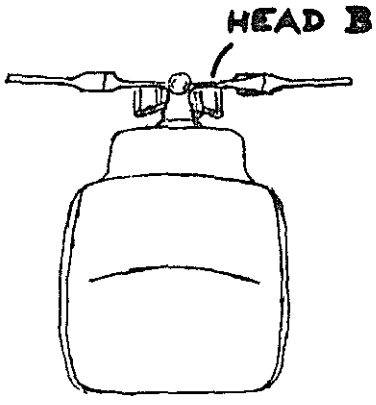

FIG. 2 TEST MODEL

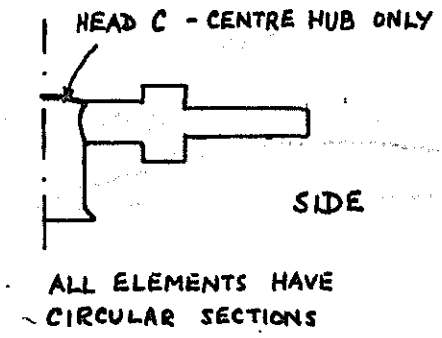

FIG. 3 HEADS A & C

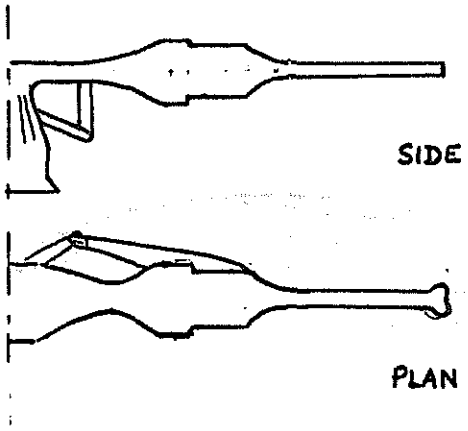

FIG. 4 HEAD B

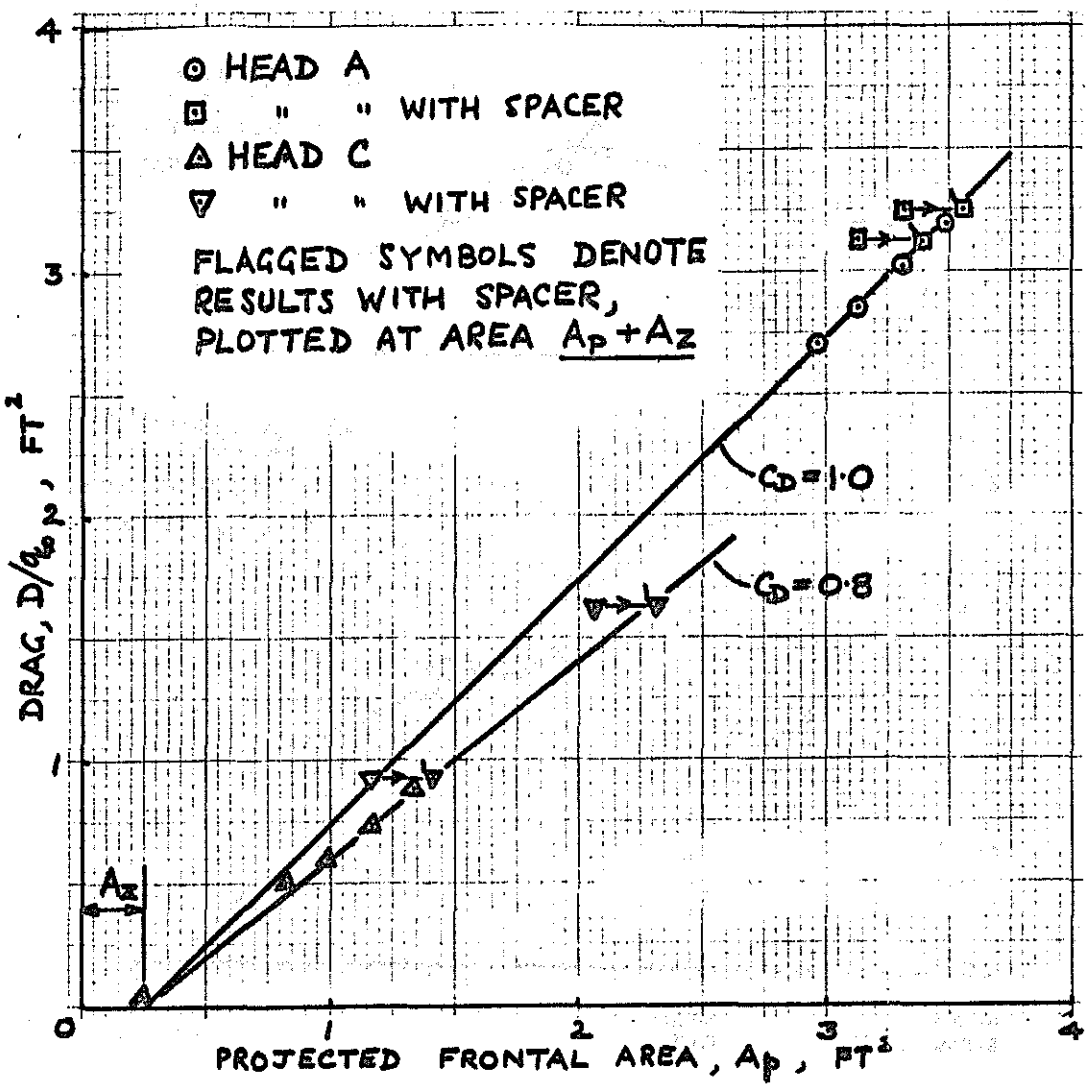

FIG. 7 HEAD DRAG MEASURED ON FLAT BOARD

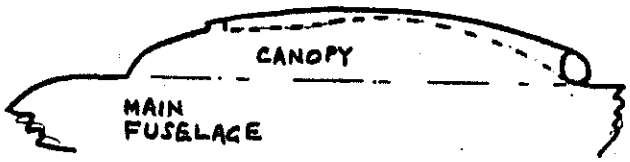

FIG. 5 CANOPY Z

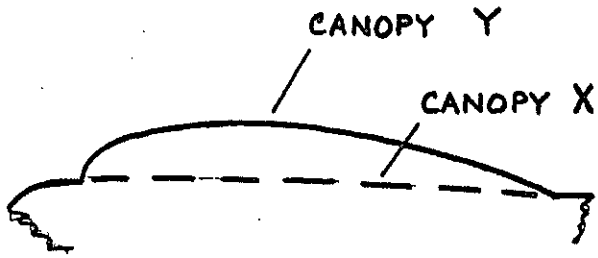

FIG. 6 CANOPIES X & Y

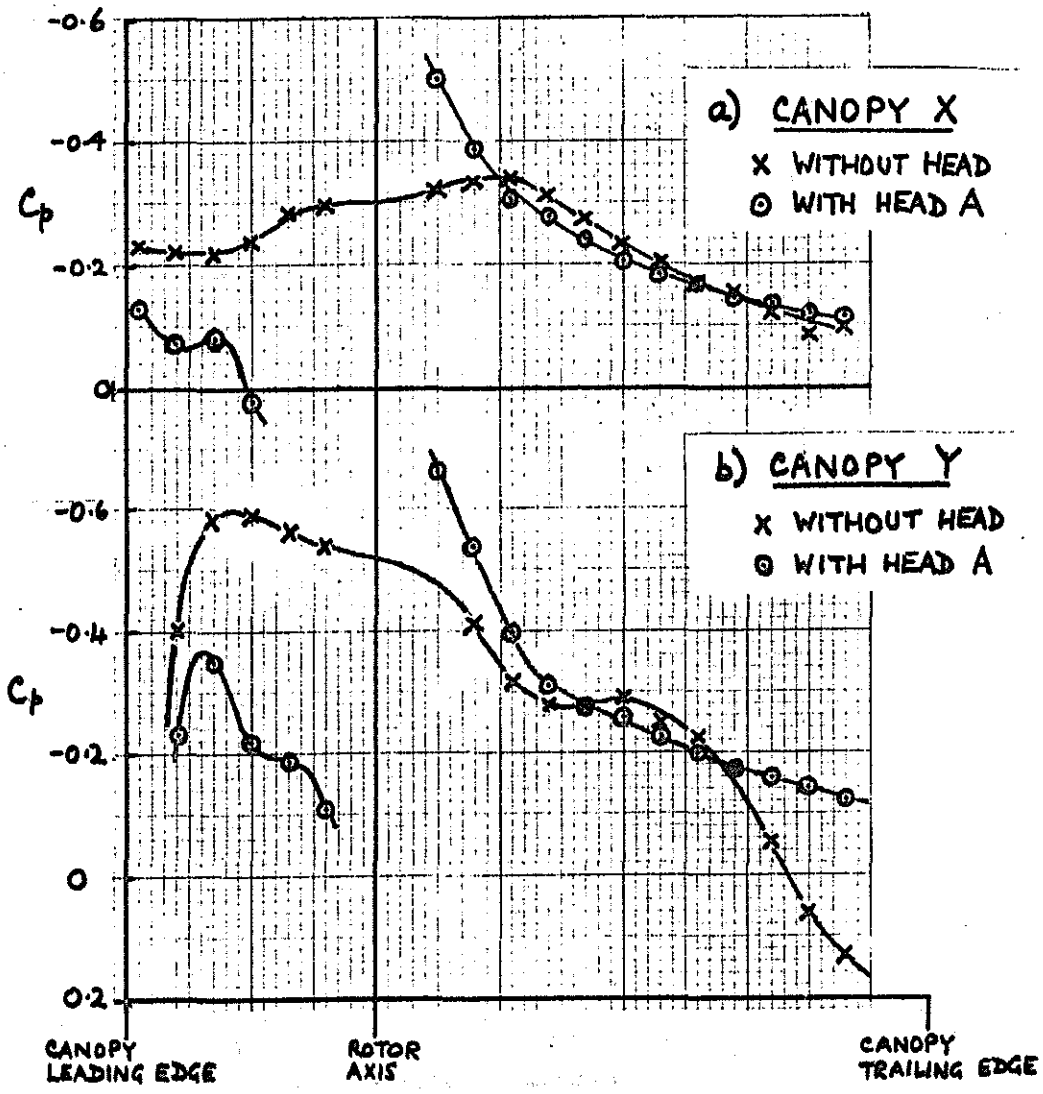

FIG. 8 SURFACE PRESSURES ON CANOPY ℄

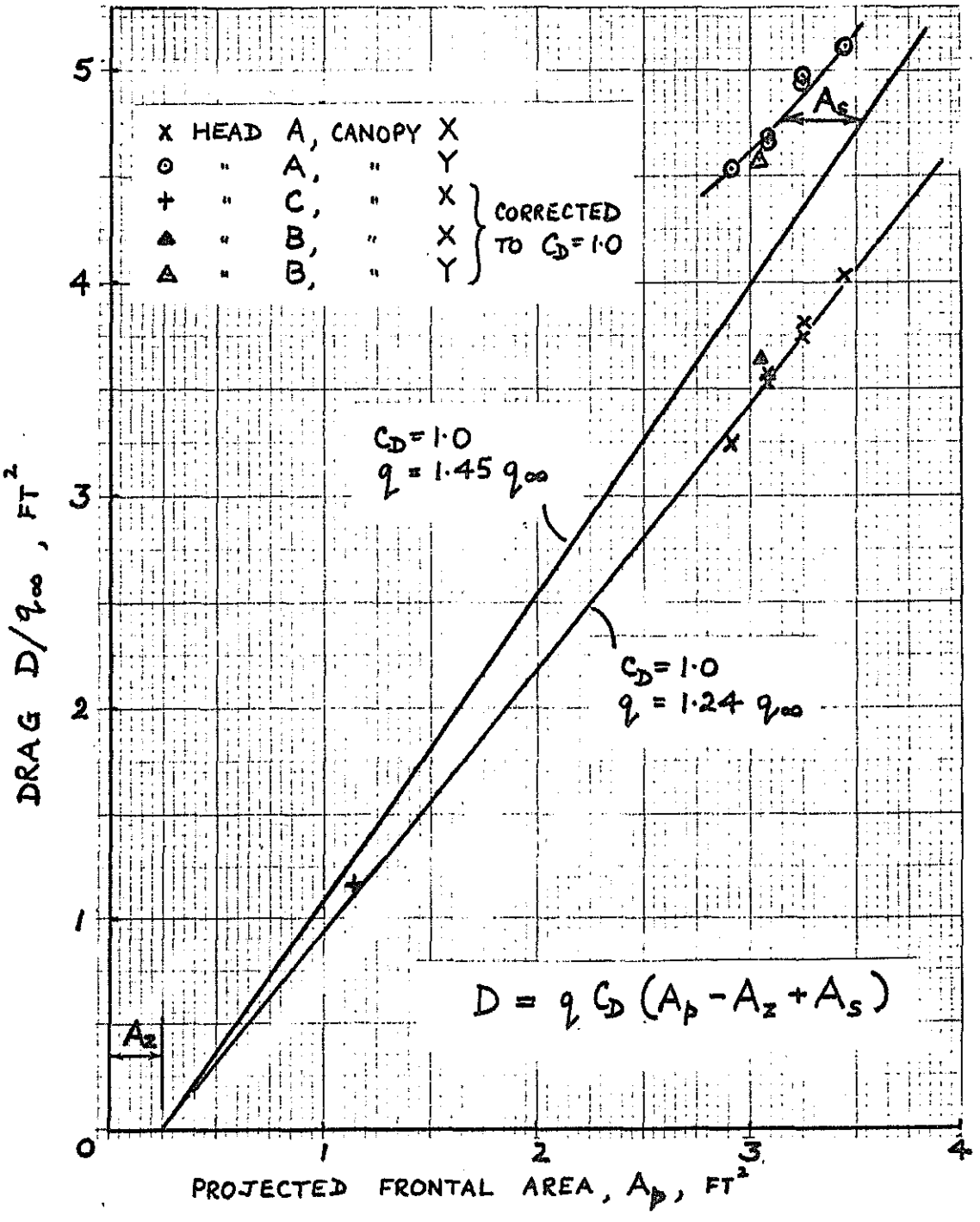

FIG. 9 HEAD DRAG MEASURED ON HELICOPTER MODEL

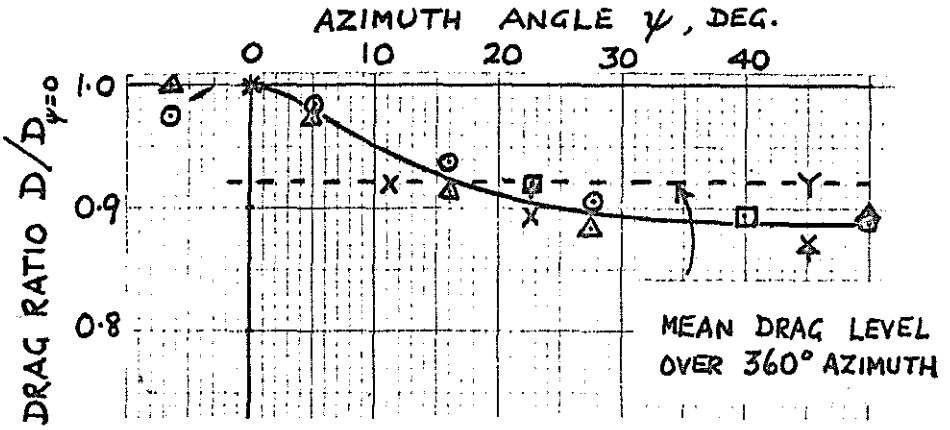

FIG. 10 EFFECT OF AZIMUTH ANGLE

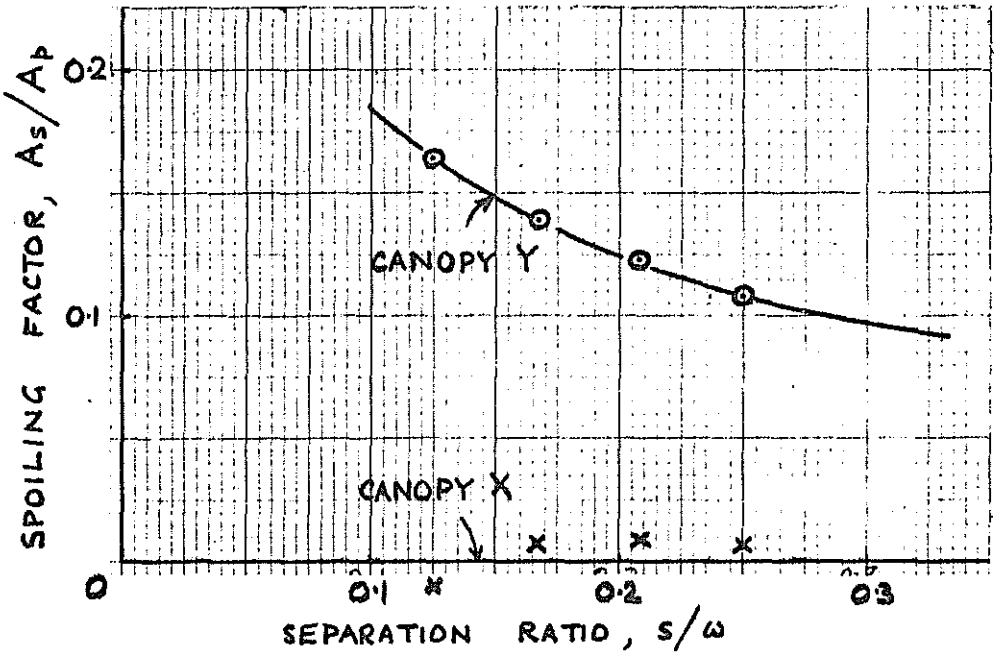

FIG. 11 FLOW SPOILING DRAG ON CANOPY

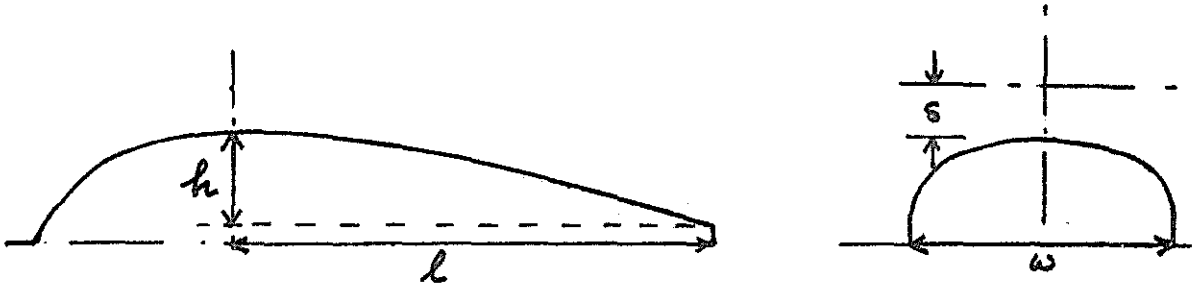

FIG. 12 CANOPY PARAMETERS